Available online at www.sciencedirect.com
ScienceDirect
Journal of Power Sources 162 (2006) 21–29
JOURNAL OF POWER SOURCES
www.elsevier.com/locate/jpowsour

# Development of alkaline direct methanol fuel cells based on crosslinked PVA polymer membranes

Chun-Chen Yang *, Shwu-Jer Chiu, Wen-Chen Chien

*Department of Chemical Engineering, Mingchi University of Technology, Taipei Hsien 243, Taiwan, ROC*

Received 1 May 2006; received in revised form 19 June 2006; accepted 19 June 2006
Available online 1 August 2006

**Abstract**

A novel crosslinked PVA/SSA (10 wt.% sulfosuccinic acid) solid polymer membrane was obtained by a solution casting technique. An alkaline direct methanol fuel cell (DMFC) is composed of an air cathode with a mixture of $MnO_2$/BP2000 + CNT binary carbon inks, a Ti-based anode electrode with PtRu black inks (varied from 0.25 to 4.50 mg cm$^{-2}$) and an alkaline crosslinked PVA/SSA solid polymer membrane. The electrochemical characteristics of the anode and cathode electrodes were investigated by the linear polarization method, cyclic voltammetry (CV) analysis, potentiostatic method and AC impedance spectroscopy. A Ti-mesh (Delker) with a thickness of 0.1 mm was used as a current collector on the anode electrode without a diffusion layer, which greatly reduced the mass transfer resistance for the electrode reaction. It was demonstrated that the alkaline DMFC using this novel crosslinked PVA/SSA solid polymer membrane showed excellent electrochemical performance at ambient temperature and pressure. The maximum peak current density of the DMFC was about 4.13 mW cm$^{-2}$ at 60 °C and 1 atm in 2 M KOH + 2 M $CH_3OH$ solution.


*Keywords:* Direct methanol fuel cell (DMFC); PVA; SSA; PtRu black; Ti-mesh; $MnO_2$

## 1. Introduction

Direct methanol fuel cells (DMFCs) [1–18] and polymer electrolyte membranes fuel cells (PEMFCs) [19–25] have recently received attention since these power sources have high-energy efficiency and a low emission of pollutants. In the case of a PEMFC, hydrogen is used as the fuel and delivers a power density of 300–500 W cm$^{-2}$ at 80–90 °C. However, using hydrogen as fuel may cause some problems due to production, storage and transportation of hydrogen. Therefore, the direct methanol fuel cell has attracted more attention than PEMFC because of use of a liquid methanol fuel, which is easy to deliver and store. More importantly, the liquid fuel can be used at ambient temperature and pressure, which makes DMFC suitable for portable 3C electronic devices [13–18].

However, the development of an acidic DMFC has faced several serious problems: (i) slow methanol oxidation kinetics [5,6], (ii) the poisoning of the catalyst by CO intermediates on the Pt surface [3,11], (iii) high methanol crossover through the membrane [7,9] and (iv) high costs of the Nafion membrane and Pt catalyst. Moreover, the electrocatalyst for methanol oxidation is still an important research issue in the development of the direct methanol fuel cell.

The Pt electrocatalyst has a low activity for methanol oxidation due to the poisoning by intermediate species, such as $CO_{ads}$. In order to enhance the activity of platinum, the Pt catalyst can be modified by the addition of a second metal, such as Ru, Mo, Sn and W [1]. The second kind of metal is more oxophilic and easily forms oxides; so oxygenated species are formed at lower potentials which promote the conversion of $CO_{ads}$ to $CO_2$ on the surface of the Pt, the so-called "bifunctional mechanism" [26].

It has been reported that methanol oxidation in alkaline media is kinetically faster than in acidic media [27–32]. Up to now, the PtRu binary catalyst has been recognized as the most promising electrocatalyst for methanol oxidation in acidic and alkaline media. In general, a supporting matrix such as carbon black and carbon nanotubes (CNTs) with a high surface area is essential to disperse the small Pt or PtRu alloy particles. Yu and Scott [29–31] used a Ti-metal mesh as an anode supporting substrate with a thickness of 0.1 mm for the Pt catalyst in an alkaline

* Corresponding author. Tel.: +886 2 908 4309; fax: +886 2 2904 1914.
*E-mail address:* ccyang@ccsun.mit.edu.tw (C.-C. Yang).

0378-7753/$ – see front matter © 2006 Elsevier B.V. All rights reserved.
doi:10.1016/j.jpowsour.2006.06.065

DMFC system. There are two advantages in using a metal mesh anode, the first one is that the mass transfer resistance of the reactant and product can be significantly reduced by direct contact of the methanol to the mesh and the membrane and the other one is the increase of the active surface area of the Pt catalyst.

Moreover, the advantage of an alkaline DMFC is that the methanol oxidation catalyst is less structure-sensitive and allows a wider selection window for catalyst materials, which can lead to the use of less expensive non-precious metal catalysts, such as Ag, Ni and $MnO_2$. One of the choices is to use a low cost air cathode electrode, which is composed of a mixture of $MnO_2$ catalysts mixed with BP2000/CNT binary carbon inks sprayed onto a Ni-foam.

Presently, perfluorosulfonate ionomer membranes, such as Nafion membrane (Dupont) are the primary membranes used in the DMFC. The commercial Nafion membranes, however, show serious methanol crossover problems [7,9], in which methanol permeates from the anode to the cathode side. The results of methanol permeation not only cause a loss of fuel but also a mixed potential at the cathode leading to a lower performance of the DMFC. Thus, for a liquid methanol fuel cell, it is imperative that the most important characteristic properties of a polymer membrane for the DMFC must have a lower methanol permeation of the liquid fuel. To meet this requirement, an alkaline crosslinked PVA polymer electrolyte membrane was prepared and used to assemble a passive-type direct methanol fuel cell.

In this work, the DMFC consisted of an air cathode electrode loaded with a low cost $MnO_2$ catalyst supported on BP2000/CNT binary carbons, an anode electrode coated with PtRu black catalysts with a loading of from 0.25 to 4.50 mg $cm^{-2}$ and a PVA/SSA solid polymer membrane [33–37], which is formed by directly blending PVA polymer with 10 wt.% sulfosuccinic acid (SSA). For the anodic methanol electrooxidation reaction, the cathodic oxygen reduction reaction (ORR) and the overall reaction of the DMFC in alkaline media can be described as follows:

Anodic reaction:

$$CH_3OH + 6OH^- \rightarrow CO_2 + 5H_2O + 6e^-,$$
$$E_a^\circ = -0.810\,\text{V (versus SHE)}, \quad (1)$$

Cathodic reaction:

$$\tfrac{3}{2}O_2 + 3H_2O + 6e^- \rightarrow 6OH^-,\ E_c^\circ = 0.402\,\text{V (versus SHE)}, \quad (2)$$

Overall reaction:

$$CH_3OH + \tfrac{3}{2}O_2 \rightarrow CO_2 + 2H_2O,\ E_{cell}^\circ = 1.21\,\text{V}, \quad (3)$$

The electrochemical characteristics of the anode and cathode electrodes were investigated by using the linear polarization method, cyclic voltammetry (CV) analysis, potentiostatic method and AC impedance spectroscopy. Additionally, the electrochemical characteristics of the novel alkaline DMFC were also investigated by using the linear polarization method; especially for the peak power density of the cell.

## 2. Experimental

### 2.1. Preparation of the anode electrode

A catalyst slurry ink was prepared by mixing 70 wt.% PtRu black catalyst powders (Alfa, HiSPEC 6000, PtRu black with 1:1 molar ratio), 25 wt.% Nafion binder (Aldrich, 5 wt.% solution), 5 wt.% PTFE binder solution (Dupont, 30 wt.% based solution) and a suitable amount of alcohol and distilled water. The resulting PtRu catalytic inks were ultrasonicated for 2 h. The PtRu black catalytic inks were dispersed onto the Ti-mesh matrix (Delker, USA) by a paint–brush to achieve a PtRu black loading of 0.25–4.50 mg $cm^{-2}$. The Ti-mesh matrix was firstly etched in 10 wt.% oxalic acid at 80 °C for 2 h followed by cleaning in acetone and IPA, and finally in distilled water before use. The as-prepared PtRu anode electrode was dried in a vacuum oven at 80 °C for 1 h.

The surface morphology of the PtRu anode electrode was sputtered with a thin layer of Au (Hitachi 1010 Ion sputter) and characterized with a scanning electron microscopy (S-2600 PC-SEM made by Hitachi Co. Ltd.). The crystallinity of the PtRu anode electrode was examined by Philips X'Pert X-ray diffractometer (XRD) with Cu Kα radiation of wavelength $\lambda = 1.54056$ Å for $2\theta$ angles between 10° and 80°.

### 2.2. Preparation of the cathode electrode

BP2000 carbon black (Cabot Ltd., Co.) with a specific surface area of 1500 $m^2\,g^{-1}$ and an average particle size of 12–15 nm was used as the raw material for the electrodes. The γ-$MnO_2$ (electrolytic manganese oxide, EMD) purchased from TOSOH (Japan) was used as an active catalyst material for the cathode. The γ-$MnO_2$ powder was prepared by a mechanical ball-milled treatment at a speed of 300 rpm for 12 h in a planetary ball miller (FRITSCH Puluerusette 7). The $MnO_2$ catalysts were weighed and put into an agate bowl together with 10 mm diameter agate balls. The weight ratio of $MnO_2$ catalysts to the ball-milled ball was 1:4. Before the ball-milled treatment, the $MnO_2$ catalysts were sintered at a temperature of 300 °C for 2 h.

The carbon slurry for the gas diffusion layer was prepared with a mixture of 70 wt.% Shawinigan acetylene black (AB50) with a specific surface area of 80 $m^2\,g^{-1}$ and 30 wt.% PTFE (Teflon-30 suspension) as a wet-proofing agent and binder. The carbon slurry ink was coated onto the Ni-foam as the current collector and then pressed at a pressure of 120 $kg_f\,cm^{-2}$. The gas diffusion layer was then sintered at 350 °C for 30 min. The active layer of the air electrode was then prepared by spraying a mixture of 15 wt.% of PTFE solution binder and 85 wt.% mixture powders composed of $MnO_2$ catalysts mixed with CNT/BP2000 binary carbons. The Ni-foam substrate was cut to the size of 1 and 8 $cm^2$. Both BP2000 and CNTs carbons were used as supporting material for the $MnO_2$ catalysts in the active layer (so-called a binary carbon supporting system).

The viscous slurry mixtures of $MnO_2$ and BP2000/CNT carbons were sprayed onto the Ni-foam by an air gun to a specified thickness of 0.3–0.4 mm. The resulting porous air

cathode electrode was dried in a vacuum oven at 120 °C for 12 h, then cooled to room temperature for further use.

### 2.3. Preparation of alkaline crosslinked PVA polymer membranes and MEA

Polyvinyl alcohol (PVA) (MW 75,000–80,000, Chang-Chung Chemicals), sulfosuccinic acid (SSA, 70 wt.% solution, Aldrich) and KOH (Merck) were used as received. The crosslinked PVA/SSA solid polymer membranes had been prepared by a solution casting method [38]. The appropriate weight ratios of the PVA and SSA (10 wt.%) were directly dissolved in distilled water with agitation for about 2 h at 90 °C. The SSA was used as a crosslinker here. After both the PVA polymer and SSA solution were completely dissolved in distilled water, the resulting viscous polymer solutions were continuously stirred until the polymer solution took on a homogeneous appearance. The resulting homogeneous solution was poured out onto a Petridish and weighed immediately, and then the excess water solvent was evaporated in a vacuum oven at 60 °C. After the evaporation, the Petridish with the PVA/SSA solid polymer membrane were weighed again. A freestanding and stable PVA/SSA solid polymer membrane was obtained and further crosslinked at 100 °C for 1 h. The crosslinked network for the PVA/SSA solid polymer membrane offers greater chemical and mechanical stability, reduces the degree of swelling and decreases the methanol crossover. The crosslinked PVA/SSA solid polymer membranes were stored in a PE bag for further testing.

The crosslinked PVA/SSA solid polymer membrane was sandwiched between the sheets of the anode electrode and the cathode electrode, and then hot-pressed at 60 °C for 100 $kg_f\,cm^{-2}$ for 5 min to obtain a membrane electrode assembly (MEA). The electrode area of the MEA was about 1 or 8 $cm^2$.

### 2.4. Electrochemical analysis

The electrochemical measurements were carried out in a conventional three-electrode cell. A large area platinum foil of 100 $cm^2$ and a Hg/HgO/1.0 M KOH electrode were used as the counter and the reference electrodes, respectively. The as-prepared PtRu anode electrode or the air cathode electrode was used as a working electrode. The cyclic voltammetry analysis of the as-prepared PtRu anode electrode was conducted between −0.80 and 0.40 V (versus Hg/HgO) with a scan rate of 5 mV $s^{-1}$ at 25 °C. The electrolyte for the anode electrode was a 2 M KOH + 2 M $CH_3OH$ solution. The electrolyte for the air cathode electrode was 8 M KOH solution. Before measurement, the anode and cathode electrodes were immersed in the above different electrolytes for at least 24 h at 25 °C. The potential sweep range for the anode electrode was set at −0.80 to 0.40 V (versus Hg/HgO). The potential sweep range for the cathode electrode was set at 0.10 to −0.80 V (versus Hg/HgO). The chronoamperometries of various Ti-based anode electrodes with different amounts of PtRu black inks were carried out at −0.40 V (versus Hg/HgO). All electrochemical measurements were performed on an Autolab PGSTAT-30 electrochemical system with GPES 4.8 package software (Eco Chemie, The Netherlands).

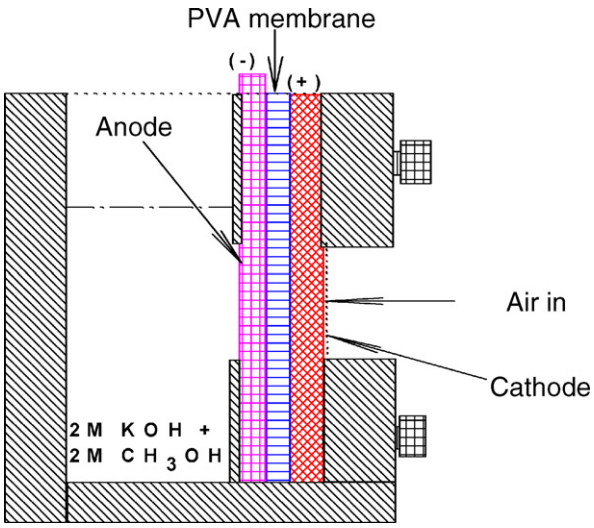


Fig. 1. Scheme of construction of test setup for a DMFC.

The AC impedance spectra of the PtRu anode electrodes were recorded with an amplitude of 10 mV in the frequency: $10^5$ and 0.01 Hz. All the measurements were carried out at ambient temperature and pressure. The electrochemical performance of a single DMFC with a low cost air cathode electrode open to the atmospheric air, were examined at a temperature between 30 and 60 °C, the construction of test setup for the alkaline DMFC is shown in Fig. 1.

## 3. Results and discussion

### 3.1. Characterization of the anode electrode

Fig. 2(a and b) shows the SEM photomicrographs for the as-received Ti-mesh and the etched Ti-mesh, respectively. Fig. 2(c and d) also shows the SEM photomicrographs for the as-prepared anode electrode with PtRu black catalysts (4.50 mg $cm^{-2}$) based on the Ti-mesh at 100× and 500×, respectively. It can be clearly seen that the Ti-mesh matrix had an open structure and exhibited a highly porous and rough metal surface after the oxalic acid etch, as shown in Fig. 2(b). The etched Ti-mesh surface obviously provides more reaction sites or contact area for PtRu black catalysts for methanol electrooxidation at the anode. Overall, as seen in Fig. 2(c and d), the PtRu black inks are uniformly sprayed onto the Ti-mesh matrix.

Fig. 3 illustrates the X-ray diffraction spectra of both the PtRu black anode electrode and the commercial E-TEK PtRu/C (Pt:Ru = 1:1 alloy (a/o) on XC72R carbon) electrode with the same catalyst loading of 4.0 mg $cm^{-2}$. All spectra of both the anode electrodes exhibit the characteristic peaks for the planes (1 1 1), (2 0 0) and (3 1 1) (absent in our XRD spectra in Fig. 3) at $2\theta$ of approximately 40°, 67° and 83°, respectively. These peaks are associated with the diffraction peaks of the fcc structure of Pt (JCPDS, card 4-802). However, all XRD peaks here are broadened and slightly shifted to higher $2\theta$ values, as observed by comparison with the peaks of Pt/C. As a matter of fact, the shift of XRD peak indicates the Ru catalyst incorporated into the Pt fcc structure of the PtRu (1:1) black catalysts and there

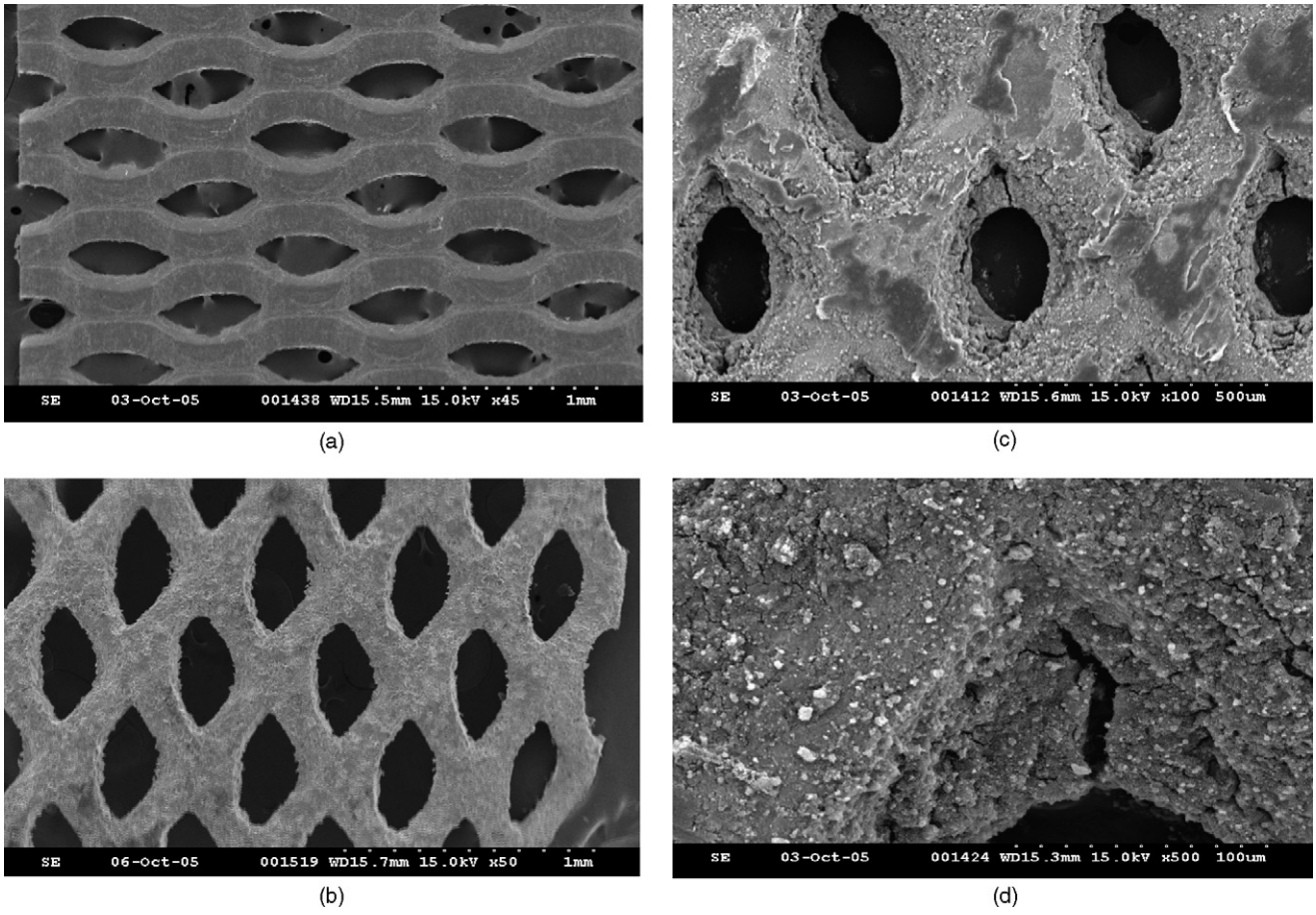


Fig. 2. SEM photographs for (a) Ti-mesh; (b) etched Ti-mesh; (c) the Ti-mesh anode electrode coated with PtRu black catalysts at 100×; (d) at 500×.

was no characteristic diffraction peak with respect to Ru (Ru has an hcp structure).

Fig. 4 shows the cyclic voltammograms of both the as-prepared PtRu anode electrode and the commercial E-TEK PtRu/C anode electrode at the same loading of 4.00 mg cm$^{-2}$ in 2 M KOH solutions at 25 °C. The peaks in the potential region between −0.80 and −0.65 V are related to the hydrogen adsorption/desorption process, whereas the anodic peaks at potentials higher than 0.0 V are related to a surface oxidation process, which represents the formation of platinum oxide. The potential region between the two peaks is the double layer region. In the

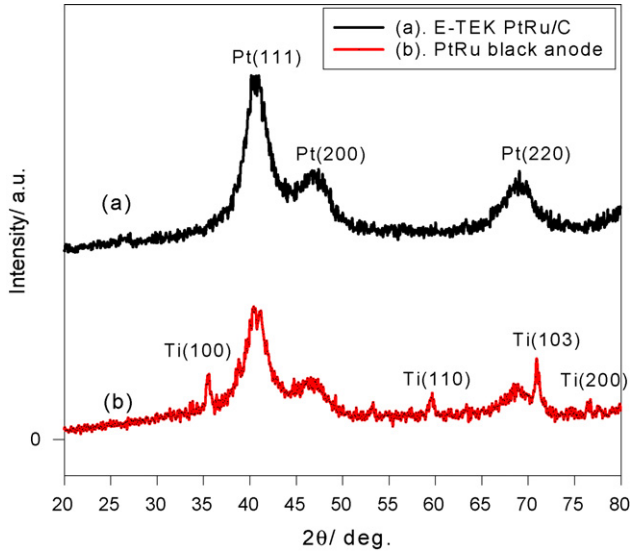


Fig. 3. XRD diffraction spectra of E-TEK PtRu/C anode electrode and the PtRu black anode electrode based on Ti-mesh at 4.0 mg cm$^{-2}$.

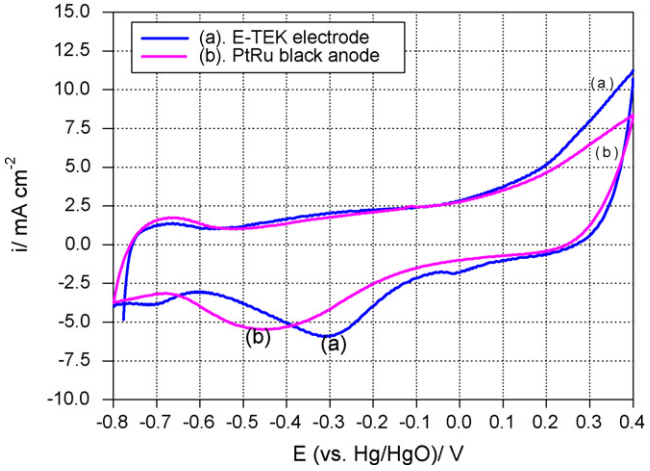


Fig. 4. Cyclic voltammograms of the as-prepared PtRu anode electrode and E-TEK PtRu/C anode electrode with a loading of 4.0 mg cm$^{-2}$ in 2 M KOH solution at a scan rate of 1 mV s$^{-1}$.

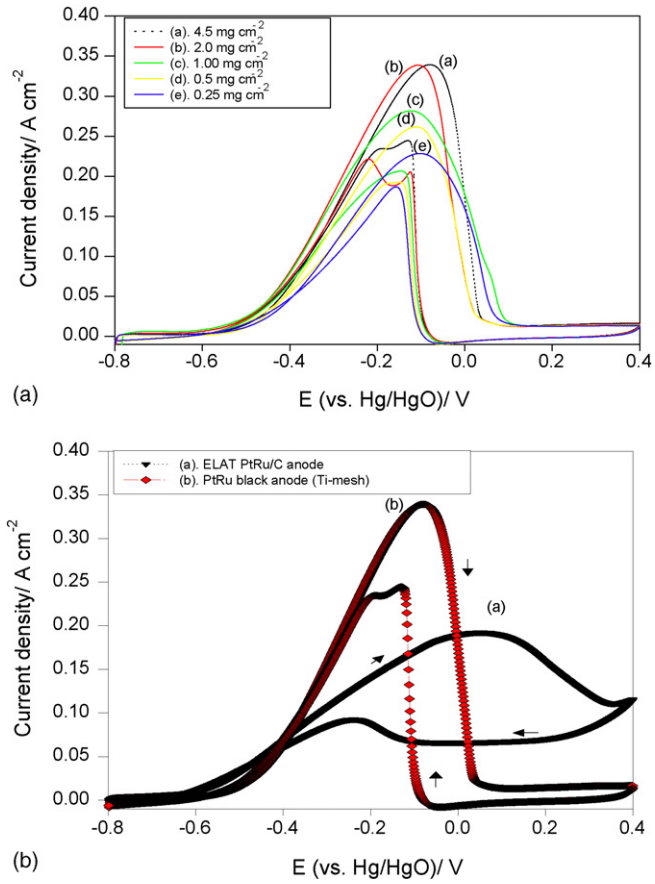


Fig. 5. Cyclic voltammograms of (a) the anode electrodes coated with various amounts of PtRu black inks; (b) E-TEK PtRu/C anode electrode in 2 M KOH + 2 M $CH_3OH$.

negative sweeping direction, a large peak appears at a potential of between −0.20 and −0.60 V, and these peaks indicate the reduction of the platinum oxide in alkaline media. Notably, the shape of the cyclic voltammograms for two anode electrodes with PtRu black and PtRu/C catalysts is similar, as observed in Fig. 4.

The cyclic voltammograms of the anode electrodes ($A = 1\ cm^2$) with different amounts of PtRu black inks with a scan rate of 5 mV $s^{-1}$ in 2 M KOH + 2 M $CH_3OH$ solution at 25 °C is shown in Fig. 5(a). The amounts of the PtRu black inks on the Ti-mesh varied from 0.25 to 4.50 mg $cm^{-2}$. The forward scanning peak potentials ($E_{p,f}$) of the methanol electro-oxidation is between −0.075 and −0.135 V (versus Hg/HgO) and the forward scanning peak current densities varies between 0.225 and 0.338 A $cm^{-2}$, as listed in Table 1. The forward peak potential seems to shift to the negative direction as the amount of PtRu black ink increases. The forward current density, however, is progressively reduced when the load of catalyst ink decreases.

Whereas, another anodic peak in the reverse scanning direction is due to the removal of incompletely oxidized carbonaceous species formed in the forward scan direction. In contrast, the reverse scanning peak potentials ($E_{p,r}$) of the methanol electro-oxidation is between −0.122 and −0.160 V (versus Hg/HgO) and the reverse scanning peak current densities is between 0.186 and 0.243 A $cm^{-2}$, as demonstrated in Table 1.

The ratio of the current densities associated with the forward anodic peak ($i_{p,f}$) and the reverse anodic peak ($i_{p,r}$) was used to evaluate the methanol oxidation electro-activity performance of the anode. The $R$ value ($R = i_{p,f}/i_{p,r}$) represents the CO tolerance of the catalysts. Accordingly, a lower value of $R$ indicates poor oxidation of methanol to CO during the anodic scan and excessive accumulation of poisoning carbonaceous species on the catalyst surface. In other words, a higher value of $R$ indicates better CO tolerance. By comparison, it was found that the as-prepared PtRu anode electrode at a load of 2.00 mg $cm^{-2}$ exhibited the best CO tolerance with $R = 1.634$ in 2 M KOH + 2 M $CH_3OH$ solution at 25 °C. On the other hand, the E-TEK PtRu/C anode electrode shows the highest CO tolerance with $R = 2.06$ for the same electrolyte solution and conditions. Nevertheless, the E-TEK PtRu/C anode electrode based on carbon fibers shows a better CO tolerance than that of as-prepared PtRu black anode electrodes based on Ti-mesh. The real reason for this difference is still not clear; and needs further study.

Fig. 5(b) also shows the result of CV analysis for the E-TEK PtRu/C anode electrode ($A = 1\ cm^2$) at a load of 4.0 mg $cm^{-2}$ at a scan rate of 5 mV $s^{-1}$ in 2 M KOH + 2 M $CH_3OH$ solution. The forward scanning peak potential ($E_{p,f}$) of the methanol electro-oxidation is at 0.05 V (versus Hg/HgO), the forward scanning peak current density ($i_{p,f}$) is about 0.192 A $cm^{-2}$ and some CV parameters are listed in Table 1. In fact, the value of $i_{p,f}$ of electro-oxidation methanol reaction of the PtRu anode electrode is about 0.338 A $cm^{-2}$ and its value is much greater than that (0.192 A $cm^{-2}$) of E-TEK PtRu/C anode electrode. By contrast, the value of $E_{p,f}$ for the PtRu anode electrode at −0.075 V is less noble than that of E-TEK anode electrode at 0.05 V. Accordingly, it can be concluded that the electrochemical performance of the Ti-based PtRu anode electrode without the gas diffusion layer

Table 1
The CV results of the Ti-based anode electrodes with various amounts of PtRu black inks in 2 M KOH + 2 M $CH_3OH$ at a rate of 5 mV $s^{-1}$

| Load (mg $cm^{-2}$) | Parameters | | | | | |
|---|---|---|---|---|---|---|
| | $E_{onset}$ (V) | $E_{p,f}$ (V) | $i_{p,f}$ (A $cm^{-2}$) | $E_{p,r}$ (V) | $i_{p,r}$ (A $cm^{-2}$) | $R$ ($=i_{p,f}/i_{p,r}$) |
| 0.25 | −0.61 | −0.102 | 0.225 | −0.160 | 0.186 | 1.20 |
| 0.50 | −0.64 | −0.120 | 0.263 | −0.140 | 0.195 | 1.34 |
| 1.00 | −0.62 | −0.135 | 0.283 | −0.150 | 0.201 | 1.41 |
| 2.00 | −0.60 | −0.100 | 0.335 | −0.122 | 0.205 | 1.63 |
| 4.50 | −0.64 | −0.075 | 0.338 | −0.125 | 0.243 | 1.39 |
| 4.00 (E-TEK) | −0.65 | 0.05 | 0.192 | −0.239 | 0.093 | 2.06 |

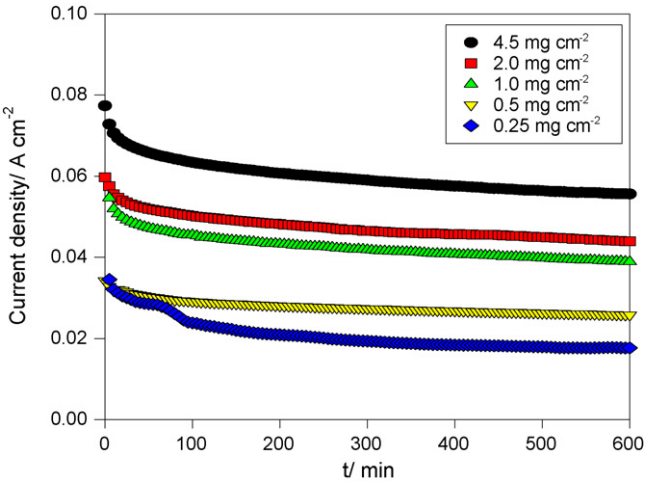


Fig. 6. Chronoamperometric curves measured at −0.40 V (vs. Hg/HgO) for the Ti-based anode electrodes with various amounts of PtRu black inks in 2 M KOH + 2 M $CH_3OH$ solution at 25 °C.

Table 2
The chronoamperometric results of the Ti-based anode electrodes with different amounts of PtRu black inks at −0.40 V (vs. Hg/HgO) for 10 h in 2 M KOH + 2 M $CH_3OH$ solution at 25 °C

| Parameter | Load (mg $cm^{-2}$) | | | | |
|---|---|---|---|---|---|
| | 0.25 | 0.50 | 1.00 | 2.00 | 4.50 |
| $i$ (A $cm^{-2}$) | 0.0176 | 0.0257 | 0.0386 | 0.044 | 0.056 |

is much better than that of E-TEK PtRu/C anode electrode with the gas diffusion layer.

Fig. 6 shows the results of the chronoamperometries at −0.40 V (versus Hg/HgO) for the anode electrodes ($A = 1\ cm^2$) coated with various amounts of PtRu black inks in 2 M KOH + 2 M $CH_3OH$ solutions. In spite of a tendency to fall at the beginning of the test, however, the current densities are stabilized and remain constant after 5 h showing good electrochemical stability for the Ti-based PtRu anode electrodes. The current densities of the Ti-based anode electrodes with different amounts of PtRu black inks can be found in Table 2. The results indicate that the best performance of the PtRu anode electrode for the methanol oxidation is at a load of 4.50 mg $cm^{-2}$.

Fig. 7 shows the AC impedance spectra of the Ti-based anode electrodes with various amounts of PtRu black inks. The $R_b$ and $R_{ct}$ parameters of the anode electrodes with various amounts of PtRu black inks are listed in Table 3. The bulk resistance of $R_b$ of the anode electrode is around 0.14–0.18 Ω. The charge transfer resistance ($R_{ct}$) of the anode electrodes varies from 2.50

Table 3
The AC parameters for the Ti-based anode electrodes coated with different amounts of PtRu black inks in 2 M KOH + 2 M $CH_3OH$ at 25 °C

| Parameters | Load (mg $cm^{-2}$) | | | | |
|---|---|---|---|---|---|
| | 0.25 | 0.50 | 1.00 | 2.00 | 4.50 |
| $R_b$ (Ω) | 0.184 | 0.150 | 0.148 | 0.159 | 0.155 |
| $R_{ct}$ (Ω) | 4.21 | 3.56 | 3.50 | 3.10 | 2.50 |

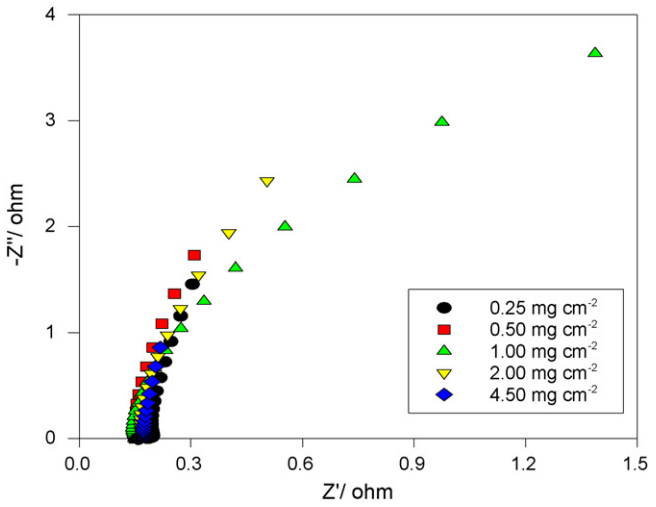


Fig. 7. AC impedance spectra of the Ti-based anode electrodes with various amounts of PtRu black inks coated on Ti-mesh in 2 M KOH + 2 M $CH_3OH$ solution at 25 °C.

to 4.21 Ω. It was revealed that the value of $R_{ct}$ of the methanol electrooxidation reaction decreases when the amount of PtRu black inks on Ti-metal mesh increases.

### 3.2. Characterization of the cathode electrode

SEM photographs for surface morphology of the active layer for the air cathode electrode sprayed with γ-$MnO_2$ catalyst supported onto CNT and BP2000 binary carbons are shown in Fig. 8(a and b) at magnifications of 500× and 7000×, respectively. Clearly, as seen in Fig. 8(b), a lot of CNT carbon aggregates are visible after $HNO_3$ acid treatment. The mixed carbon agglomerates with a mixture of CNTs (fiber) and BP2000 carbons (small round particles) are also clearly seen. There are no large PTFE clumps or PTFE fibers formed. The surface morphology of the active layer exhibited a nonuniform pancake shape, as shown in Fig. 8(a). The $MnO_2$ catalyst for the ORR was actually supported by two different characteristic carbons; the first one is with a higher electric conductivity and lower surface area of CNT carbons (100–300 $m^2\ g^{-1}$) and the other one has a higher surface area of the BP2000 carbon black (1500 $m^2\ g^{-1}$). In order to enhance the electrocatalytic activity of the $MnO_2$, the oxide catalysts were firstly treated by a mechanical ball-miller and then annealed at 300 °C for 2 h. In general, the ball-milled treatment was used to get more amorphous and nanocrystalline structures for the materials. Moreover, the addition of carbon nanotubes as a secondary support provided a large surface area, good electronic conductivity and fast kinetics for the oxygen reduction reaction.

Fig. 9(a) shows the linear polarization curves of the air electrodes ($A = 1\ cm^2$) with various amounts of carbon slurries which contain $MnO_2$ catalyst carbons in 8 M KOH solutions at 25 °C with a scan rate of 1 mV $s^{-1}$. The loading of catalyst carbon slurries varied from 0.63 to 3.63 mg $cm^{-2}$ through a multiple spray technique. It can be clearly seen from Fig. 9(a), the reduction current density of the air electrode with $MnO_2$/binary carbon inks at a loading of 3.63 mg $cm^{-2}$ at −0.50 V (versus Hg/HgO)

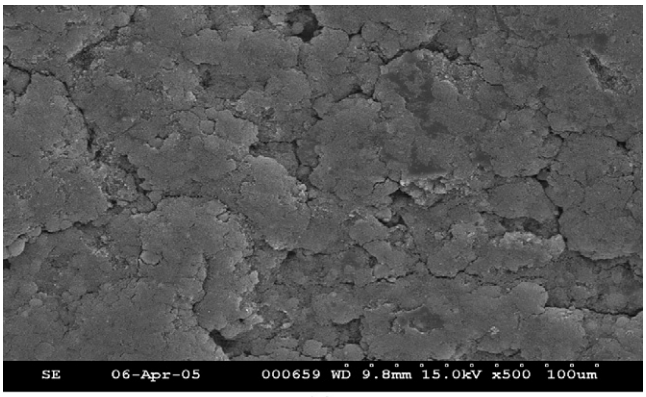


Fig. 8. (a and b) SEM photographs of the air electrode with $MnO_2$/BP2000 + CNTs inks on Ni-foam.

is about $-440.2\,mA\,cm^{-2}$ (Table 4). It was apparent that an increase of the thickness of the active layer greatly enhanced the electrocatalytic activity of the air electrode. It was also observed that the electrochemical performance of the air electrodes was similar, as $MnO_2$/binary carbon inks are in the range between 0.63 and 2.45 $mg\,cm^{-2}$.

Notably, the electrochemical performance of the air electrode with $MnO_2$/binary carbon inks at 3.63 $mg\,cm^{-2}$ was greatly enhanced. In fact, the characteristic properties of two carbon materials for the air electrodes are significantly different. The specific surface area of BP2000 (1500 $m^2\,g^{-1}$) carbon black is six times greater than that of conventional Vulcan XC-72R (250 $m^2\,g^{-1}$) carbon black. The higher surface area of BP2000 greatly increased the number of reaction sites for $O_2$ reduction.

Furthermore, it is well known that the bulk resistance of the $MnO_2$ catalyst powders is high and the addition of CNT materials improves the electronic conductivity of the air electrode. As CNTs have a hollow tubular structure and contain many micro- or nano-sized pores, the active layer was more easily penetrated by the KOH electrolyte solution through the capillary action. The highly conductive CNTs bridge the separated conductive carbon channels and result in an increase in the electronic conductivity of the air electrode. The appropriate amounts of CNTs as secondary substrate mixed with $MnO_2$ powders indeed help improve the electrochemical performance of the air electrode.

Fig. 9(b) shows the linear polarization curves of the air electrode ($A = 1\,cm^2$) loaded with $MnO_2$ catalyst inks at a loading level of 3.63 $mg\,cm^{-2}$ for ORR in 1, 4 and 8 M KOH concentrations at 1 $mV\,s^{-1}$. It was experimentally discovered that the current density of the ORR of the air electrode in 8 M KOH solutions is much greater than that of the air electrode in 1 and 4 M KOH solutions. The most possible reason is that the 8 M KOH solutions have a higher ionic conductivity or higher concentration of charge carriers than 1 and 4 M KOH solutions.

Table 4
The *I–V* values of the air electrodes with ball-milled $MnO_2$ catalyst supported on CNT/BP2000 (1:1) binary carbons in 8 M KOH solutions at 25 °C

| *E* (vs. Hg/HgO) (V) | *i* ($mA\,cm^{-2}$) | | | |
|---|---|---|---|---|
| | 0.63[a] | 1.40[a] | 2.45[a] | 3.63[a] |
| −0.10 | −1.22 | −3.18 | −1.94 | −16.5 |
| −0.20 | −6.62 | −16.4 | −14.8 | −91.5 |
| −0.30 | −16.50 | −40.2 | −42.5 | −201.3 |
| −0.40 | −28.7 | −68.7 | −77.5 | −320.5 |
| −0.50 | −44.5 | −105.3 | −123.3 | −440.2 |
| −0.60 | −63.2 | −148.1 | −175.6 | −561.8 |
| −0.70 | −84.0 | −192.7 | −229.5 | −689.7 |

[a] Loads ($mg\,cm^{-2}$).

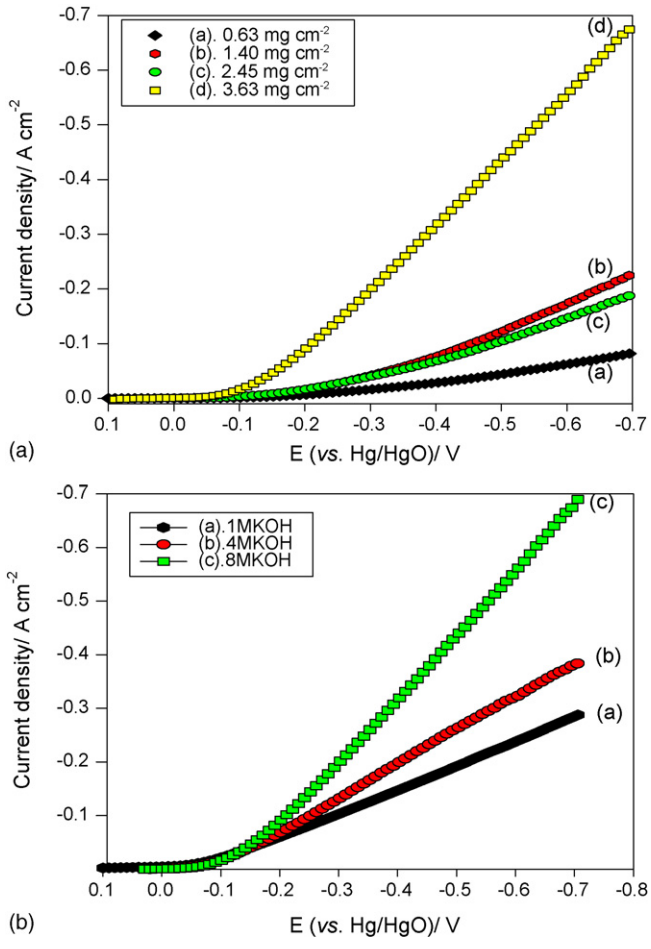


Fig. 9. The cathodic polarization curves of the air electrodes (a) at various loads; (b) in different concentrations of KOH solutions at 25 °C at 1 $mV\,s^{-1}$.

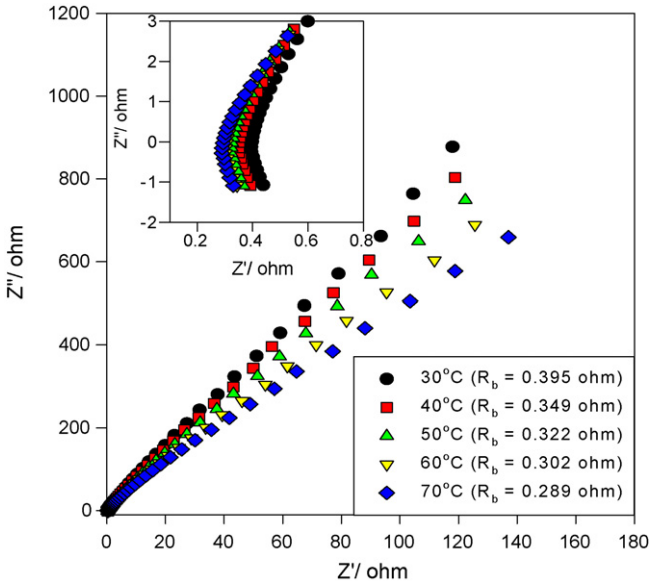


Fig. 10. AC spectra of alkaline PVA/SSA polymer electrolyte membranes at various temperatures.

### 3.3. Characterization of the alkaline crosslinked PVA/SSA solid polymer membranes

The AC impedance spectra of alkaline crosslinked PVA/SSA solid polymer membrane (SSA used as a crosslinker) at different temperatures are illustrated in Fig. 10. Before the ionic conductivity measurement, a suitable size of a crosslinked PVA/SSA solid polymer membrane was immersed in a 8 M KOH solution for at least 24 h at ambient temperature. The AC spectra are typically non-vertical spikes for blocking electrodes, i.e., SS |PVA/SSA SPE| SS cell. Typical AC impedance spectra show two well-defined regions. The high frequency range AC spectra, which are related to the ionic conduction process in the bulk of the solid polymer electrolyte membrane, can be obtained. In the low frequency range, a straight line parallel to the imaginary axis that is attributed to the effect of the blocking electrode was found.

Since the blocking electrode is used in impedance analyses, the electrolyte/electrode interface can be regarded as a capacitance. When the capacitance is ideal, it should show a vertical spike in an impedance diagram. However, the inclined spike at an angle ($\theta$) less than 90° is found instead of the vertical spike. This is known to come from the non-homogeneous or roughness of the electrolyte/electrode interface. Analysis of the AC spectra yields information about the properties of the PVA/SSA solid polymer electrolyte such as bulk resistance ($R_b$). The bulk resistance can be calculated from the intercept on the higher frequency side on the $Z_{re}$ axis. The obtained $R_b$ value is converted into the ionic conductivity of PVA/SSA solid polymer membrane, $\sigma$, using the equation $\sigma = L/R_bA$, where $L$ is the thickness (cm) of alkaline crosslinked PVA/SSA solid polymer membrane, $A$ the area of the blocking electrode ($cm^2$) and $R_b$ is the bulk resistance (Ω) of alkaline polymer membrane. The geometric surface area of the stainless steel blocking electrode was 0.785 $cm^2$.

Table 5
The ionic conductivities of alkaline crosslinked PVA/SSA solid polymer membranes at different temperatures

| $T$ (°C) | Parameters | | |
|---|---|---|---|
| | $L$ (cm) | $R_b$ (Ω) | $\sigma$ (S $cm^{-1}$) |
| 30 | 0.013 | 0.395 | $4.19 \times 10^{-2}$ |
| 40 | 0.013 | 0.349 | $4.74 \times 10^{-2}$ |
| 50 | 0.013 | 0.322 | $5.14 \times 10^{-2}$ |
| 60 | 0.013 | 0.302 | $5.48 \times 10^{-2}$ |
| 70 | 0.013 | 0.289 | $5.73 \times 10^{-2}$ |

The values of $R_b$ for alkaline crosslinked PVA/SSA solid polymer membranes are typically in the range of 0.3–0.5 Ω, as shown in the inset of Fig. 10, and are dependent on the composition of the sample film, post-crosslinked temperature and time. The value of ionic conductivity is of the order of $10^{-2}$ S $cm^{-1}$. Table 5 shows the conductivity values of alkaline crosslinked PVA/SSA solid polymer membranes (crosslinked at 100 °C for 1 h) at different temperatures. The temperature dependence of the ionic conductivity of alkaline crosslinked PVA/SSA solid polymer membranes is of the Arrhenius type [33–37]. The $\log_{10}(\sigma)$ versus $1/T$ plot, not shown here, obtains the activation energy ($E_a$) of alkaline PVA/SSA solid polymer membrane, which is dependent on the membrane compositions and the degree of the crosslinking conditions. The $E_a$ value for alkaline crosslinked PVA/SSA solid polymer membrane is in the range of 5–10 kJ $mol^{-1}$. Also, it was experimentally revealed that the 8 M KOH electrolyte absorptions for the crosslinked PVA/SSA solid polymer membranes are in the range of 35–42 wt.%.

### 3.4. Electrochemical characterization of a single DMFC

Fig. 11 shows the potential–current density curves and power density–current density curves of the DMFC containing an

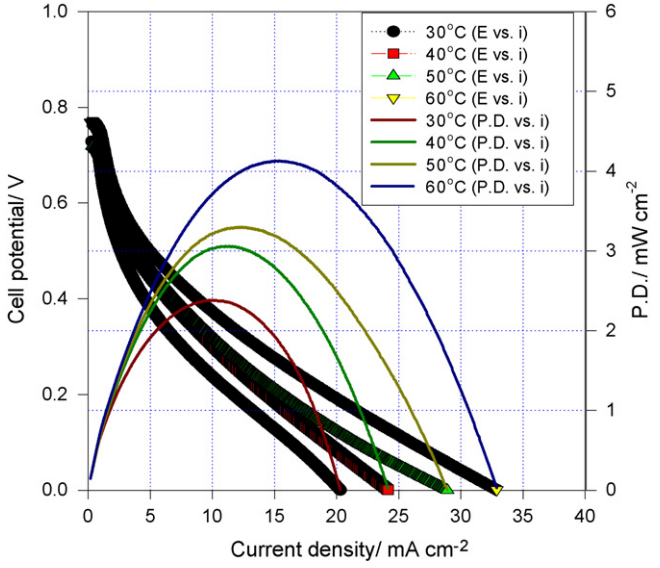


Fig. 11. Cell potential and power density as a function of the current density for a DMFC with crosslinked PVA/SSA solid polymer membrane in 2 M KOH + 2 M $CH_3OH$ solution at ambient pressure at various temperatures.

Table 6
The electrochemical parameters for the alkaline DMFC with the crosslinked PVA/SSA solid polymer membrane in 2 M KOH + 2 M $CH_3OH$ at 1 atm at different temperatures

| Parameters | $T$ (°C) | | | |
|---|---|---|---|---|
| | 30 | 40 | 50 | 60 |
| $E_{ocp}$ (V) | 0.729 | 0.769 | 0.779 | 0.768 |
| $E_{p,max}$ (V) | 0.245 | 0.269 | 0.278 | 0.268 |
| $i_{p,max}$ (mA cm$^{-2}$) | 9.73 | 11.36 | 11.86 | 15.41 |
| $PD_{max}$ (mW cm$^{-2}$) | 2.38 | 3.06 | 3.30 | 4.13 |

anode electrode ($A = 8\,cm^2$) with PtRu black at a loading level of 4.50 mg cm$^{-2}$, a cathode electrode with $MnO_2$/binary carbon inks with a loading level of 3.63 mg cm$^{-2}$ and a crosslinked PVA/SSA solid polymer membrane at temperatures between 30 and 60 °C in 2 M KOH + 2 M $CH_3OH$ solution at ambient pressure (1 atm). The maximum power density of 2.38 mW cm$^{-2}$ was achieved at $E_{p,max} = 0.245$ V with a peak current density ($i_{p,max}$) of 9.73 mA cm$^{-2}$ at 30 °C. On the other hand, a maximum power density of 4.13 mW cm$^{-2}$ was obtained at $E_{p,max} = 0.268$ V with a peak current density of 15.41 mA cm$^{-2}$ at 60 °C. Table 6 lists some electrochemical parameters such as the open circuit potential ($E_{ocp}$), the maximum power density ($PD_{max}$), the peak potential ($E_{p,max}$) and the peak current density ($i_{p,max}$) at different temperatures for the alkaline DMFC. It was found that the values of the open circuit potential of the alkaline DMFC were about 0.75–0.79 V. As a result, the maximum powder density of the alkaline DMFC increased as the operational temperature increased.

## 4. Conclusions

A novel alkaline direct methanol fuel cell composed of the crosslinked PVA/SSA solid polymer membrane was assembled and examined. The electrochemical characteristics of the anode and cathode electrodes were individually investigated by using the linear polarization method, cyclic voltammetry analysis, potentiostatic method and AC impedance spectroscopy. In particular, a Ti-metal mesh substrate was chosen for the anode electrode without the gas diffusion layer, so the liquid methanol can easily reach the three-phase interface zone and the mass transfer resistance of the electrode reactions was greatly reduced. It was demonstrated that the DMFC with this novel crosslinked PVA/SSA solid polymer membrane showed excellent electrochemical performance at ambient temperatures and pressures. The maximum peak power density of the DMFC was about 4.13 mW cm$^{-2}$ at 60 °C and 1 atm. From the DMFC application point of view, this alkaline DMFC composed of a low cost air cathode electrode (i.e., $MnO_2$ is a non-precious metal catalyst), a Ti-based PtRu anode electrode and a PVA/SSA solid polymer membrane (PVA is a cheap polymer) is a low cost system. In this work, we demonstrated that the PVA/SSA solid polymer membrane was a potential candidate for DMFC applications.

## Acknowledgements

Financial support from the National Science Council, Taiwan (Project no.: NSC-94-2214-131-002) is gratefully acknowledged. It is very appreciated that Delker Company (USA) kindly offers the Ti-mesh samples for this work.

## References

[1] W.H. Lizcano-Valbuena, V.A. Paganin, E.R. Gonzalez, Electrochim. Acta 47 (2002) 3715.
[2] N. Nakagawa, Y. Xiu, J. Power Sources 118 (2003) 248.
[3] G.G. Park, T.H. Yang, Y.G. Yoon, W.Y. Lee, C.S. Kim, Int. J. Hydrogen Energy 28 (2003) 645.
[4] H. Fukunaga, T. Ishida, N. Teranishi, C. Arai, K. Yamada, Electrochim. Acta 49 (2004) 2123.
[5] V. Baglio, A.S. Arico, A.D. Blasi, V. Antonucci, P.L. Antonucci, S. Licoccia, E. Traversa, F.S. Fiory, Electrochim. Acta 50 (2005) 1241.
[6] T.C. Deivaraj, J.Y. Lee, J. Power Sources 142 (2005) 43.
[7] S. Panero, P. Fiorenza, M.A. Navarra, J. Romanowska, B. Scrosati, J. Electrochem. Soc. 152 (2005) A2400.
[8] K. Furukawa, K. Okajima, M. Sudoh, J. Power Sources 139 (2005) 9.
[9] J.H. Choi, Y.M. Kim, J.S. Lee, K.Y. Cho, H.Y. Jung, J.K. Park, I.S. Park, Y.E. Sung, Solid State Ionics 176 (2005) 3031.
[10] V.S. Silva, S. Weisshaar, R. Reissner, B. Ruffmann, S. Vetter, A. Mendes, L.M. Madeira, S. Nunes, J. Power Sources 145 (2005) 485.
[11] B.E. Hayden, D.V. Malevich, D. Pletcher, Electrochem. Commun. 3 (2001) 395.
[12] E. Antolin, Mater. Chem. Phys. 78 (2003) 563.
[13] G.Q. Lu, C.Y. Wang, J. Power Sources 144 (2005) 141.
[14] C.Y. Yang, P. Yang, J. Power Sources 123 (2003) 37.
[15] T. Shimizu, T. Momma, M. Mohamedi, T. Osaka, S. Sarangapani, J. Power Sources 137 (2004) 277.
[16] K. Kordesch, V. Hacker, U. Bachhiesl, J. Power Sources 96 (2001) 200.
[17] J.G. Liu, T.S. Zhao, R. Chen, C.W. Wong, Electrochem. Commun. 7 (2005) 288.
[18] B.K. Kho, I.H. Oh, S.A. Hong, H.Y. Ha, Electrochim. Acta 50 (2004) 781.
[19] P. Costamagna, S. Srinivasan, J. Power Sources 102 (2001) 242.
[20] C. Wang, Z.X. Liu, Z.Q. Mao, J.M. Xu, K.Y. Ge, Chem. Eng. J. 112 (2005) 87.
[21] H. Chang, J.R. Kim, J.H. Cho, H.K. Kim, K.H. Choi, Solid State Ionics 148 (2002) 601.
[22] R. Benitez, J. Soler, L. Daza, J. Power Sources 151 (2005) 108.
[23] R. Fernandez, P. Ferreira, L. Daza, J. Power Sources 151 (2005) 18.
[24] A. Ayad, J. Bouet, J.F. Fauvarque, J. Power Sources 149 (2005) 66.
[25] R. Thangamuthu, C.W. Lin, J. Power Sources 150 (2005) 48.
[26] M. Watanabe, S. Motoo, J. Electroanal. Chem. 60 (1975) 275.
[27] A.V. Tripkovic, K.D. Popovic, B.N. Grgur, B. Blizanac, P.N. Ross, N.M. Markovic, Electrochim. Acta 47 (2002) 3707.
[28] A.V. Tripkovic, K.D. Popovic, J.D. Lovic, V.M. Jovanovic, A. Kowal, J. Electroanal. Chem. 572 (2004) 119.
[29] E.H. Yu, K. Scott, J. Power Sources 137 (2004) 248.
[30] E.H. Yu, K. Scott, Electrochem. Commun. 6 (2004) 361.
[31] E.H. Yu, K. Scott, R.W. Reeve, J. Electroanal. Chem. 571 (2003) 17.
[32] F. Colmati, V.A. Paganin, E.R. Gonzalez, J. Appl. Eelectrochem. 36 (2006) 17.
[33] C.C. Yang, J. Power Sources 109 (2002) 22.
[34] C.C. Yang, S.J. Lin, J. Power Sources 112 (2002) 497.
[35] C.C. Yang, S.J. Lin, Mater. Lett. 57 (2002) 873.
[36] C.C. Yang, S.J. Lin, J. Appl. Eelectrochem. 33 (2003) 777.
[37] G.M. Wu, S.J. Lin, C.C. Yang, J. Membr. Sci. 275 (2006) 127.
[38] J.M. Rhim, H.B. Park, C.S. Lee, J.H. Jun, D.S. Kim, Y.M. Lee, J. Membr. Sci. 238 (2004) 143.